A Model for the Structure of MCM-41 Incorporating Surface Roughness

Chandrashekhar G. Sonwane, Christopher W. Jones, and Peter J. Ludovice*

School of Chemical & Biomolecular Engineering, Georgia Institute of Technology, 311 Ferst Drive, Atlanta, Georgia 30332

Received: April 4, 2005; In Final Form: August 16, 2005

The surface area of MCM-41 mesoporous silica, estimated by several models in the literature, is significantly less than the value derived from BET analysis of nitrogen adsorption at 77.4 K. In the past, the difference has been attributed to several reasons including the errors involved in the BET analysis of the multilayer-capillary condensation region and the heterogeneity of the walls. In the present work, we present an alternate model of MCM-41 based on molecular simulations that gives surface area values that are in closer agreement to those determined by experiment. The model incorporates bulk heterogeneity of the material, surface hydroxyls, and most importantly, physical deformations or indentations of the pore surface. The model predicts small-angle X-ray diffraction (XRD) and wide-angle X-ray scattering (WAXS) results that are consistent with experimental data as well as surface areas and pore volumes that compare favorably with published experimental results. The simulation results are consistent with the hypothesis that the interstitial space in MCM-41 is relatively amorphous despite the regular arrangement of the mesopores. The surface roughness associated with the amorphous structure increases the surface area beyond the nominal value produced by assuming smooth cylindrical pores.

1. Introduction

Ordered mesoporous materials such as MCM-41[1] are used in a variety of applications because of their unique features.[2,3] They contain an array of uniformly sized pore channels that form a non-networked pore structure with negligible pore blocking. The diameters of these hexagonally packed mesopores can be precisely tuned between 2 and 15 nm by suitable modification of the pre- or postsynthetic procedure.[4] The materials have high thermal, hydrothermal, and mechanical stability.[5−8] They also possess a very narrow pore-size distribution, a high surface area (∼1000 m^2/g), and a high pore volume (∼0.8 cm^3/g), estimated via analysis of the cryogenic nitrogen adsorption isotherm. The surface properties can be easily modified by depositing guest species on the surface or in the silicate framework.[2,3] Currently, MCM-41 materials are being used in catalysis,[2] size-exclusion filtration,[9] nanowire fabrication[10] membranes,[11,12] adsorption,[13] and as a support for enzymes,[14] among other applications.

Literature reports suggest that the cross section of these pores in MCM-41 may be hexagonal[15] or circular.[1] Often, these materials are referred to as crystalline, where the term crystalline refers to the regular arrangement of mesopores in a hexagonal pattern. Traditionally, crystallinity refers to the regular arrangement of atoms in a unit lattice. However, these materials (MCM-41) are neither completely crystalline nor amorphous.[1,16] In contrast, acidity measurements of aluminosilicate MCM-41 as well as X-ray diffraction studies indicate that the silicate in the walls is more like amorphous silicates than crystalline materials.[16] In this work, to avoid confusion, we use the term noncrystalline to refer to the arrangement of atoms in the MCM-41 walls and the term ordered structure to refer to the regular arrangement of the mesopores.

Several reports indicate that MCM-41 materials do not always have the ideal, uniform hexagonal arrangement of cylindrical pores that was originally proposed. For example, transmission electron microscopy (TEM) and scanning electron microscopy (SEM) have revealed that some samples of MCM-41 contain channels that are substantially curved.[17,18] Additionally, there are several reports using theoretical as well as experimental analysis that indicate that the surface of MCM-41 is rough and heterogeneous.[16−20] Fenelenov and co-workers[19] provided a quantitative estimate of surface roughness by defining a roughness coefficient, β. The value $\beta = 1$ corresponds to the smooth surface, whereas values higher than 1 indicate increased roughness. For MCM-41, they used gas-adsorption analysis and synchrotron X-ray diffraction and found that $\beta = 1.1-1.2$. Additionally, TEM as well as fractal analysis using gas-adsorption isotherms indicated that the surface of MCM-41 is very rough.[17,20] Although there is no conclusive evidence that the surface indentations in the walls are so significant that they result in interconnecting channels between the mesopores, the recent synthesis of CMK-3 materials using MCM-41 as a template indicates that in some cases this may occur.[21,22] CMK-3 materials are carbon-based materials made by filling in the mesopores of ordered silicates. Interconnecting channels seem to be required to keep the resulting carbon cylinders from collapsing on themselves; however, this interconnection of the carbon cylinders in CMK-3 may result from the processing of the CMK-3 materials as opposed to the presence of interconnecting micropores in MCM-41. On the basis of t-plot analyses, Branton and co-workers[23] suggested that the micropores in the wall of MCM-41 that interconnect the mesopores were absent, an observation that was later verified by Kruk et al.[24] However, on the basis of the effect of trimethylsilylation of surface silanols on the adsorption of water, pyridine, *n*-hexane, and cyclohexane, Long et al.[25] suggested that micropores of approximately 0.5 nm diameter were present in the walls of their MCM-41 samples. It is interesting that the presence of micropores in the walls of SBA-15 interconnecting the mesoporous channels of

* Corresponding author. E-mail: pete.ludovice@chbe.gatech.edu.

10.1021/jp051713c CCC: $30.25
Published on Web 11/18/2005

the material has been verified.[26−31] SBA-15 is fabricated using triblock copolymers instead of alkylammonium surfactants (as used in MCM-41).[26] They too have a hexagonal arrangement of uniformly sized cylindrical mesopores. However, they have a larger pore size (5−30 nm) and thicker walls (~3 nm or more). TEM and gas-adsorption isotherm (t-plot) analyses have clearly indicated that SBA-15 has micropores in the walls.[27−31] The degree to which significant surface roughness exists in the pores of MCM-41 may explain why measurements of the effective surface area are much higher than those calculated by assuming that the walls of the pores are smooth. Therefore, any simulation of the effective surface area must accurately account for such surface roughness.

There have been several attempts to model the structure of MCM-41 materials in the past.[32−51] The validity of the models has been most often tested by comparing simulated gas-adsorption studies and small-angle-powder X-ray diffraction (XRD) patterns with experimental results. Rarely are surface area and pore volume used as metrics, despite the discrepancy between the nominal surface area, which assumes a perfectly smooth surface and pore volume (estimated from the geometry of the pores), and the actual values determined from adsorption experiments. We hypothesize that the inclusion of the appropriate level of surface roughness is of critical importance in reconciling this difference with simulation. Therefore, a detailed review of the previous models is merited to highlight the variety of methodologies used and the level of agreement/discrepancy with experimental data. A detailed review of these models is provided in section 2.

We have an interest in developing a model for MCM-41 for simulated studies of tethered catalytic groups in such mesoporous hosts. Indeed, molecular catalysts tethered within mesoporous hosts have been widely studied,[53−63] and in some cases, the encapsulation of catalysts in the mesoporous structure results in enhanced catalytic properties.[53] On the basis of an analysis of the existing literature, we believe that a suitable model for such an application does not exist. In developing a model for MCM-41, we identified several criteria that would lead to a realistic structure: (1) Regular arrangement of pores − the simulated material has an arrangement of mesopores that matches experimental XRD and TEM results closely. (2) Arrangement of atoms − the simulated material has a similar arrangement of atoms in the bulk and surface, and the arrangement is in line with data from experimental techniques such as WAXS and measured surface hydroxyl concentrations. (3) Structural characteristics − the surface area and pore volume match the experimental gas-adsorption results reasonably well.

In this work, a new model for the structure of MCM-41 that incorporates surface roughness is proposed. The model is a modification of the procedure used by Feutson and Higgins[35] that incorporates roughness in the walls, bulk heterogeneity, and surface hydroxyls to account for the surface roughness believed to exist in MCM-41. Given the paucity of evidence for microchannels that interconnect the mesopores, we will not include interconnecting micropores in the model. The simulated surface area, pore volume, and XRD patterns are compared with experimental values from the literature.

2. Previous Simulations of MCM-41

The models of MCM-41 used in the literature can be broadly classified into three main categories.

2.1. Approximate Models Considering MCM-41 as a Smooth Tube or Cylinder. Seaton and co-workers[38,39] used a series of models based on cylindrical tubes. In the first model, He and Seaton[38] inserted a regular array of oxygen atoms in three concentric layers. The second model is based on the α-quartz crystal structure with a skeletal density of 2.66 g/cm^3. A block of α-quartz was constructured, and cylindrical tubes were created by removing the atoms whose centers do not reside in the cylindrical annulus. Although the orientation of the pore relative to the unit cell of the quartz may be of importance, this effect was not reported in the paper. In the third model, they placed Si and O atoms randomly using stochastic simulations. Si and O atoms in a ratio of 1:2 were generated in a cylindrical simulation box with the following restrictions: (1) a maximum of four oxygen atoms within 1.65 Å of a silicon atom and (2) a maximum of two silicon atoms within 1.65 Å of an oxygen atom. The atoms were then allowed to adjust in the simulation box during an energy minimization. The pore length was kept at 4 nm, and periodic boundary conditions were applied in the direction parallel to the pore. They found that the third model (stochastic model) gave the most accurate results in predicting the adsorption of ethane, carbon dioxide, and a binary gas mixture of the two.

Denoyel and co-workers[43] modeled MCM-41 as an array of oxygen atoms in a cylindrical annulus with each atom interacting with an adsorptive atom via a Lennard-Jones (LJ) 6−12 potential. Although the wall was made from only oxygen atoms, the interaction with adsorbates is nonhomogeneous in such a way that the energetic and surface heterogeneity are defined as a distribution rather than a fixed value. For the adsorption of Ar and Kr modeled via the grand canonical Monte Carlo simulation (GCMS), they found that the energy-site distribution determines low-pressure adsorption, whereas the structural distribution affects multilayer adsorption.

Cao and co-workers[44] used a cylindrical pore model to represent MCM-41. Using GCMS and density functional theory (DFT), they found a good comparison between the simulation and experiments for the adsorption isotherm of nitrogen at 77 K, as well as that for carbon tetrachloride and methane at 273 K. For both GCMS and DFT models, the MCM-41 pores were assumed to be smooth cylindrical tubes consisting of one atomic layer.

The earliest work of Neimark and co-workers[48] and work by Bhatia and co-workers[49] represented the MCM-41 pores as cylindrical tubes.

2.2. Models Obtained by Analyzing Experimental Small-Angle XRD Results. White and co-workers[32] developed a model that assumes that the interstitial space near the pores is lower in density than the rest of the silicate. On the basis of X-ray diffraction using high-intensity synchrotron radiation, they proposed that MCM-41 of ca. 4 nm pore diameter (4.6 nm spacing between pores and a wall thickness of ~0.6 nm) consists of a two-layer wall structure as shown in Figure 1. The models used for Figure 1 will be discussed later in sections 2 and 3. The inner hollow pore has a 6.89 Å radius, which is surrounded by a first wall layer of 0.87 g/cm^3 density up to a radius of 19.69 Å. The second layer has a density of 0.99 g/cm^3 and exists in the rest of the material beyond the radius of 19.69 Å from the center of each pore.

Solovyov and co-workers[41] modeled the structure of MCM-41 using techniques similar to those used by Edler and co-workers,[32] reporting that along with a continuous electron density distribution the modeling of synchrotron X-ray plots could provide important structural and geometrical information such as wall thickness and pore shape and size. They have reported that the walls of MCM-41 are not continuous and

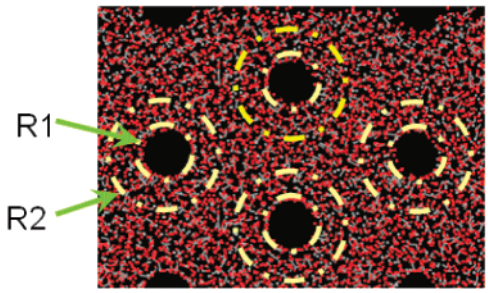

Figure 1. Structural model proposed by Edler and co-workers.[32] In the present work, their model has been simulated using two different approaches. This represents the unoptimized structure.

smooth and that there is a possibility of gaps/holes in the walls. Their findings support the idea that the walls of MCM-41 may possess some surface roughness.

2.3. Models Using a Hexagonal or Cubic Arrangement of Pores. Feutson and Higgins[35] used classical molecular dynamics (MD) to study MCM-41 materials with a series of lattice constants and wall thicknesses. To represent the micelles used in the experimental synthesis, they filled the cylindrical pore inside a hexagonal unit cell with Lennard-Jones atoms with closed-packed structure. They fixed these atoms during the entire simulation. After the pseudo-micelles were placed in the MD cell, the Si and O atoms were inserted using two different approaches. In the first approach, the Si atoms were randomly inserted between the cylinders with a density close to that of vitreous SiO_2, being careful not to place any two Si atoms within 2.5 Å of each other. Oxygen atoms were then placed between all neighboring pairs of Si atoms. In the second approach, cylindrical sheets of SiO_2, similar in structure to carbon fullerene straws, were placed around the pseudo-micelle. In this way, the SiO_2 is ordered near the pore surface but disordered in the center of the walls. In both approaches, the initial structures were allowed to reach thermal equilibrium using a three-body potential. Feutson and Higgins found that the simulated diffraction pattern for materials formed from amorphous silica with walls thicker than 11 Å was in excellent agreement with experiment. It was reported that the silanol concentrations of all simulated structures were in agreement with the values observed in vitreous silica. Vitreous or glassy silica is believed to be more amorphous than the walls of MCM-41 (as discussed later in the article). Also, it is possible that the fraction of silanols is higher in vitreous silica than in MCM-41.

Koh and co-workers[36,37] developed a model that involves the insertion of Si and O atoms randomly inside a unit cell of the size determined by XRD, until the correct wall density is obtained. They used two criteria to decide if each randomly generated position was acceptable: the atom position is not within the free volume of the pore and not within 3 Å of any of the other atoms. Hydrogen atoms were then placed randomly on the surface. They used the models to study the separation of CH_2Cl_2 from nitrogen. They found that the simulated values of selectivity for CH_2Cl_2 were significantly higher than the experimental results. Koh and co-workers[37] also used the model to study the removal of carbon dioxide from a CO_2/CH_4 mixture. They found huge discrepancies between the experimental and simulated separation factors. In both cases, they attributed the discrepancies in part to the poor choice of the model for MCM-41.

Schuth and co-workers,[40] to assess the significance of XRD and TEM images, constructed computer models of amorphous silica with a 1D pore system and hexagonally arranged pores. They found that the simulated TEM images obtained depended strongly on the imaging conditions. They studied the possibility of deformations in the walls by introducing several deformities by physically moving the atoms in the unit cell. Utilizing simulated XRD patterns of the deformed MCM-41 models, they found that deformation in the hexagonal cell or broadening of the pore size distribution had an insignificant effect on the XRD patterns. This confirms that XRD patterns alone may not necessarily provide the best tool for defining the degree of order in the regular arrangement of the pores.

Sauer and co-workers[42] used a two-step approach to simulate the structures of yttria-coated SBA-15 and MCM-41 materials. In the first step, a unit cell was generated from SiO_2, and a weighted random placement of atoms was used to simulate a distribution of atoms inside the cell forming a continuous, smooth transition from pore to wall. In the second step, the structure factors and the intensities of reflections were calculated. They found a good comparison between the experimental and simulated intensities of the powder diffraction patterns.

Coasne and Pellenq[45] modeled the structure of MCM-41 materials by starting with a cristoballite cube with a cylindrical pore running through it. All of the Si atoms that were present in an incomplete tetrahedral environment were removed. After removing dangling atoms and hydroxylating unpaired oxygens, they displaced the atoms in the cube to obtain structures that have a hexagonal or elliptical cross section. They found that there was no effect of pore size on the argon adsorption isotherm for pores larger than 10 nm. For pores smaller than 6 nm, the thickness of the adsorbed layer increases with decreasing pore size at a given pressure. While studying the effect of surface roughness on adsorption, they found that adsorption in a rough pore can be described as a sum of the adsorbed amount in a similarly sized smooth pore and a constant contribution due to atoms trapped in the pits and indentations comprising the additional surface roughness. While studying the effect of pore shape, Coasne and Pellenq found that inside hexagonal and ellipsoidal smooth pores the gas/adsorbate interface retained the memory of the pore shape and became cylindrical prior to capillary condensation. The film thickness in a hexagonal pore was close to that of a cylindrical pore of similar dimension. However, the film thickness for an ellipsoidal pore was always larger than that for an equivalent cylindrical pore.

Kleestorfer and co-workers[46] modeled MCM-41, starting with a block of α-quartz and making a cylindrical hole inside it. They found that with decreasing wall thickness the lattice energy decreases until a pore size is reached where the walls become partially disconnected at their thinnest sections. They also found that the formation of interconnections between pores was energetically highly unfavorable. They determined that the walls were noncrystalline and that the pores were slightly hexagonal.

Maddox and Gubbins[47] used a model that considered only oxygen atoms randomly placed in a unit cell (with the cylindrical annulus at the center and quarter pores at each corner of the lattice) to form an amorphous array with only repulsive and dispersive interactions (without any partial charges). They assumed that the low polarizability of silicon atoms leads to negligible dispersion interactions. They used a skeletal density of 2.7 g/cm^3, which is close to the density of quartz (2.66 g/cm^3) and is significantly higher than that of MCM-41 as well as that of amorphous silica (2.2 g/cm^3). They suggested that modeling a single unit cell may be sufficient, because the LJ potential decays to a negligible amount over a few nanometers. They reported that a 1D homogeneous potential gave rise to a poor prediction of the adsorption isotherm at low pressure (nitrogen

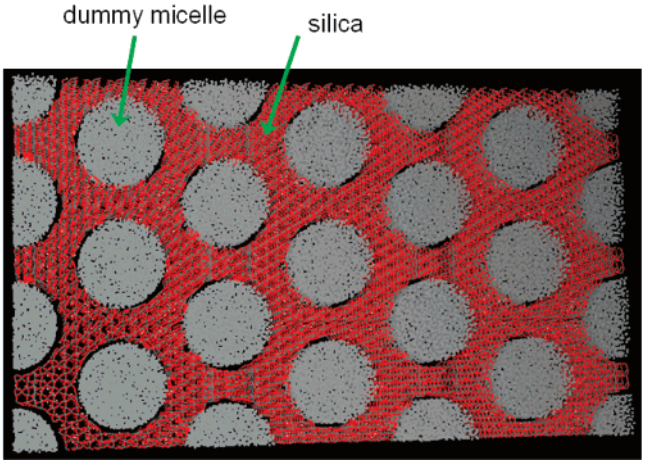

Figure 2. 3 × 3 × 1 structure of MCM-41 simulated in the present work showing the dummy atoms and the silicate network.

adsorption at 77.4 K). A heterogeneous potential with a 2D solid−fluid potential that greatly fluctuated around the pore wall gave excellent agreement for low-pressure adsorption data. They suggested that the wall thickness of MCM-41 could be on the order of 2.5−6 Å. The model was able to predict the pore size and adsorption isotherms accurately.

3. New Simulation of MCM-41

3.1. Arrangement of Bulk Atoms. *Method 1*. The basic procedure in the present model follows the work of Feutson and Higgins.[35] However, several modifications have been made to make the model more realistic. Figure 2 shows a 3 × 3 unit cell of a structure that has been simulated here. To represent micelles, a tube or a cylinder filled with randomly placed dummy atoms is used to create modeled micelles. One hexagonal unit cell model consists of one cylindrical modeled micelle (as shown in Figure 2) at the center of the cell and four-quarters of a modeled micelle at the corner of the unit cell. The dummy atoms representing the modeled micelle were frozen during the entire simulation. In the simulations, the modeled micelles will have LJ interactions with the atoms in the walls. The dimensions of a unit cell are 7.928 × 4.577 × 3 nm^3, representing the width, height, and thickness of the unit cell. Periodic boundary conditions were used with *P*1 symmetry. The length of the pore simulated by Feutson and Higgins[35] was 1 nm, which we thought was too small for future applications of this model as a host for a tethered catalyst. Therefore, we used a value of 3 nm.

Following the approach of Seaton and co-workers,[38,39] the silica was inserted inside the cell using two different approaches. In the first approach, Si and O atoms in a ratio of 1:2 were placed in the unit cell in such a way that the atoms formed a regular quartz lattice, surrounding a pore 3.5 nm in diameter. A fixed degree of amorphousness was introduced into the silica structure by randomly breaking 1−5% of the randomly selected bulk Si−O bonds and turning the terminal oxygen into a hydroxyl group and adding a hydroxyl group to the terminal silicon. These broken bonds were applied only to silicon atoms that were at least 1.5 Å away from the pore surface. The degree of amorphousness was controlled by the fraction of bonds that were remodeled. The surface roughness was controlled by introducing a known number of physical deformations into the pore surface. Physical deformations were created by removing the atoms from randomly selected spherical areas, approximately 4−6 Å in diameter, from the entire cell until the skeletal density was about 2.2 g/cm^3. The diameters of these spherical voids were chosen from a Gaussian distribution with a mean of 5 Å and a standard deviation of 1 Å. A skeletal density of 2.2 g/cm^3 has been used by several researchers[20,24,35] in the past and appears to be representative. Because the wall thickness in many of the simulated structures is less than 1 nm, the addition of these spherical voids mainly impacts the surface of the mesopores.

Method 2. In an alternate approach, Si and O atoms in 1:2 stoichiometry were inserted sequentially at random positions inside the unit cell consisting of modeled micelles using a set of rules to avoid the formation of O−O and Si−Si bonds. Before placing a new atom, the following checks were made: (a) The silicon is not surrounded by more than four oxygen atoms. (This refers to a sphere with a radius equal to a bond length of 1.65 Å or less around each silicon atom.) (b) The oxygen atoms are not surrounded by more than two silicon atoms. (c) The two silicon atoms cannot be closer than the bonding distance of 2.33 Å. (d) Two oxygen atoms are not within a distance of 1.48 Å from each other. The structure was then equilibrated as described below. Additonal details of this placement procedure are provided in the literature.[38,39]

3.2. Surface Hydroxyls. The experimentally observed surface concentration of hydroxyl groups strongly depends on preparation and treatment conditions. Jentys and co-workers[64] have reported that their samples of MCM-41 have 0.79 mmol/g of weakly acidic surface OH groups (samples were synthesized using C_{16}TMABr as SDA, calcined at 813 K, and then air dried for 8 h). Zhao and co-workers[65] reported that ca. 2 to 3 silanol groups per nm^2 are present on the surface of MCM-41, using NMR. (For a material with a surface area of 800 m^2/g, this corresponds to ∼3 mmol/g.) We have used the estimate 0.79 mmol/g in the present work. To achieve this, the unpaired O atoms on the surface of the tube were protonated. The bulk of the material present in the walls (about 0.15 nm from the surface) was not considered for protonation because it was assumed that it does not contribute to the surface hydroxyls. The structure was then minimized using molecular mechanics in the molecular operating environment (MOE) from the Chemical Computing Group.[66]

3.3. Optimization. The nonlinear optimization algorithm used in MOE[66] was used to minimize the modeled structure such that the rms average of the elements of the Cartesian gradient vector were less than 0.01 kcal/mol Å. MOE uses a sequential series of steepest descent (SD), conjugate gradient (CG), and truncated Newton (TN) algorithms for energy minimization.[67] SD minimization was applied until either 100 iterations or an rms average energy gradient of 1000 kcal/mol Å was reached. The CG method was then applied until either 100 iterations or an rms average energy gradient of 1000 kcal/mol Å was reached, followed by the TN method until the final rms gradient target was reached.

Several force fields such as MMFF94x,[68] CHARM22,[69] and Amber94[70] were used for the model relaxation. It was found that the MMFF94x force field gave radial distribution functions closest to those obtained from the experimental WAXS results; therefore, it was used for all of the simulations here. The structure was heated to 500 K and equilibrated for about 200 ps before it was cooled down to 300 K using NVT simulations. The NVT algorithm used in MOE is the Nose−Poincare algorithm,[71] integrated by the generalized leapfrog algorithm.[72,73] This was coded by making slight changes in the MOE formulation using the scientific vector language (SVL) in MOE. This Nose−Poincare formation is symplectic and limits the

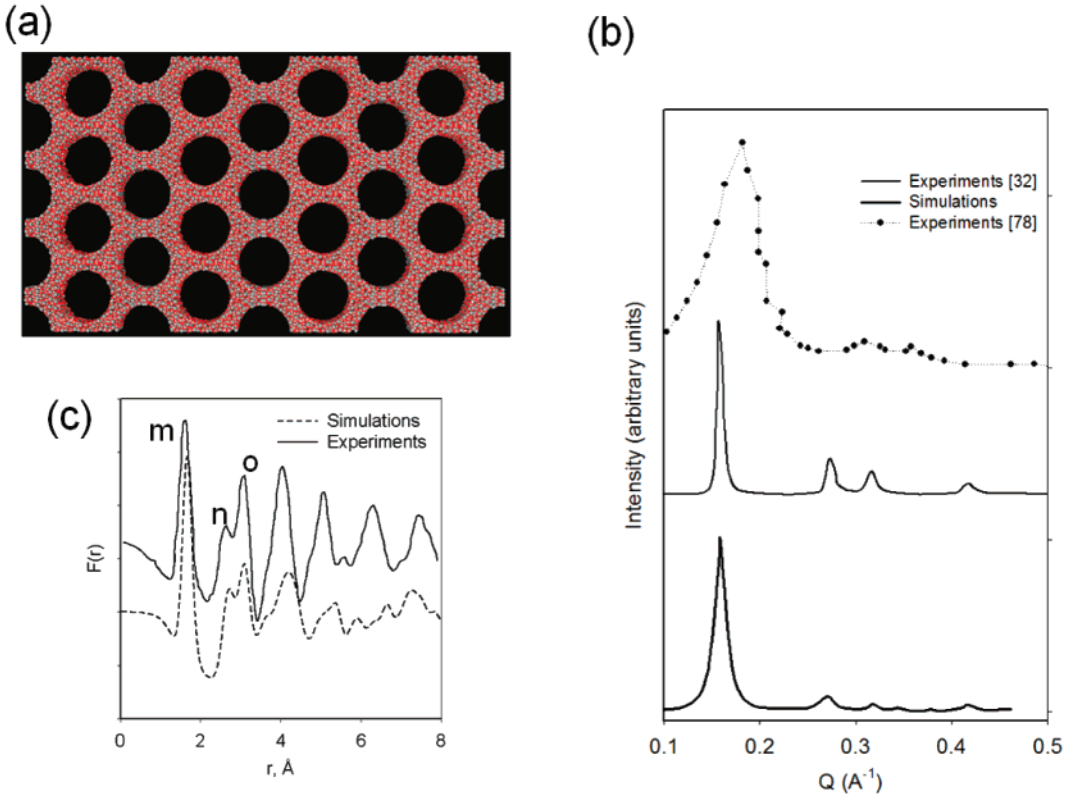

Figure 3. Characterization of the model developed in the present work. (a) Superstructure consisting of 16 unit cells (4.577 nm lattice spacing and 3.5 nm pore diameter). (b) Experimental[32] and simulated X-ray diffraction patterns plotted vs the magnitude of the scattering vector **Q**, simulated: model (solid line), ref 32 (bold line), and ref 78 (dotted line). (c) Experimental[78] and simulated reduced electronic density distribution function from WAXS.

growth of the artificial perturbation due to the thermostat algorithm. The step size was 2 fs, and the heating was carried out over 100 ps.

3.4. Accessible Surface Area. The accessible surface area of the models was estimated using Connolly's procedure.[74] Because of the high density and low temperature of cryogenic nitrogen adsorption, a GCMS of this process is computationally demanding. Therefore, we used the Connolly surface as a computational expedient. In the Connolly method, there are three kinds of surfaces that form the accessible surface area of the probe radius. They are patches of spherical-convex, spherical-concave, and torus-saddle surfaces. These pieces of surfaces form a connected network, covering the molecule. This is analogous to a polyhedron, except that it is curved. The two surfaces join at an edge/arc, and two arcs join at vertexes. The joining of the two surfaces is smooth and has a well-defined tangent plane. In this aspect, Connolly surfaces are better than van der Waals surfaces because in the latter there are sharp crevices where atoms intersect. In practice, the probe sphere of a predefined diameter is rolled over the surface of the structure. The Connolly surface is traditionally used to study the accessibility of the aqueous phase inside biological molecules. The application of this method to get the accessible surface area (to compare it with the area obtained from the adsorption) of the porous material requires a spherical approximation of the adsorbate molecule (usually a nitrogen molecule at 77 K inside the pores). The estimates of the Connolly surface area were obtained using the Cerius2 software program.[74] We believe that the Connolly surface reasonably represents the surface of the spherical atoms present in the adsorbed phase, given that the approximation that a mean spherical approximation of nitrogen (3.68 Å used in the present work[75]) is accurate. To the best of our knowledge, the only other example of the application of the Connolly method for porous materials is the study of porous tin selenides by Ahari and co-workers.[77]

4. Results and Discussion

Recognizing that the term MCM-41 represents a class of mesoporous materials with different pore diameters and surface areas, a single simulation cannot accurately characterize the entire class of materials. This is an important issue when dealing with structures prepared with the same surfactant template but different sources of silica or synthesis conditions. Ideally, one could test a single, well-characterized material and compare the experimental data to simulated results. Unfortunately, it is rare that one finds a paper that characterizes a single sample in sufficient detail to allow the comparison of small-angle XRD patterns, adsorption isotherms with pore volume and surface area, wide-angle XRD patterns with radial distribution functions (RDFs), surface hydroxyl concentrations, et cetera. In particular, there is only one published report of a RDF for MCM-41.[78] To that end, our simulated material is compared to data from several research papers, although care was taken to ensure that all the data came from samples that were synthesized using C_{16}TMA surfactants as structure-directing agent generating material. Experimental values are derived from the following literature reports: XRD patterns,[32,78] TEM images,[15] RDFs,[78] pore volumes,[19,32] and surface areas.[17,32,33,47,80]

4.1. Arrangement of Mesopores. Figure 3a shows the 4 × 4 × 1 lattice of MCM-41 material simulated in the present work using method 1. The cell dimensions are 7.928 × 4.577 × 3 nm^3, and the pore diameter is 3.5 nm. The hexagonal lattice shows a good resemblance to the TEM results reported in the literature.[15] The comparison of simulated to experimental X-ray diffraction patterns of mesoporous silicate materials is shown

in Figure 3b. The experimental data were taken from Edler and co-workers,[32] with a *d* spacing of 3.9 nm (made using a C_{16} bromide salt surfactant template and sulfuric acid), and from Fuess and co-workers,[78] with a *d* spacing of 3.5 nm (made using a C_{16} chloride surfactant). The simulated diffraction pattern was produced from the MOE program from the Chemical Computing Group.[66] The calculation assumed a Lorentzian peak shape and utilized a polarization correction assuming 50% polarization and a global Debye−Waller thermal broadening factor for all atoms. A root-mean-squared spherical value for the Debye−Waller factor of $\langle u^2 \rangle^{1/2} = 0.2$ was used, which was based on the results from Pasquarello's studies of vitreous silica.[79]

The XRD pattern in Figure 3b from the model compares well with the results from both White[32] and Fuess.[78] The results from Fuess are shifted slightly toward the higher angles to reflect the fact that this structure has a pore diameter of approximately 3.5 nm relative to the 3.9 nm pore diameter of the structure from White. This is likely due to slight differences in the synthesis procedure between the two MCM-41 samples. The model results reproduce the White[32] results better, despite the use of a nominal pore diameter of 3.5 nm in constructing the model. We attribute this apparent increase in the pore diameter to the effect of the surface roughness in the model. Despite these minor differences in the pore arrangement, we assume that the atomic structure within the walls is similar between these two samples. Therefore, we will compare the atomic structure of the walls to the Fuess sample, despite the minor difference in the pore diameter. The variation in the breadth of the diffraction peaks in Figure 3b between the two experimental samples, is likely due to the higher resolution obtained by White and co-workers because they used synchrotron radiation as opposed to the conventional diffractometer used by Fuess and co-workers. The slight variation in peak shape between White's experimental sample and our simulated results is likely due to our choice of a single global isotropic Debye−Waller factor. Diffraction studies on vitreous silica suggest that there is some anisotropy to this thermal motion, but this has not been studied in MCM-41.[79]

4.2. Wall Structure. The arrangement of the pores in MCM-41 materials is quite structured; however, much less is known regarding the structure of the interstitial space between these pores. Maddox and co-workers,[47] on the basis of their helium porosimetry measurements, suggested it to be quartz-like walls with a skeletal density of 2.7−3 g/cm^3. This value is significantly higher than the experimental skeletal density of ∼2.2 g/cm^3, reported elsewhere in the literature.[20,24] This experimentally determined density strongly suggests that the silica between the pores is amorphous, given that the density of amorphous silica is also 2.2 g/cm^3. On the basis of the broad range of Si−O−Si angles and OH groups present (20% of Si present as Si−OH, with a ±10% error), using solid-state NMR, Beck and co-workers[1] reported that MCM-41 consists of a partially crystalline or amorphous silica. The structure of the silica in the interstitial space will have a significant effect on the structure of the walls. This, in turn, will help determine the effective surface area, so it is imperative that this interstitial structure be accurately reproduced by any model attempting to determine the effective surface area of these materials.

To determine the interstitial structure of these materials properly, a reasonable metric would be to compare simulated RDFs to experimental RDFs derived from WAXS powder patterns. The RDF functions in this work were estimated using version 4.2 of the Cerius2 program from Accelrys Inc. The comparison of RDFs obtained from experimental WAXS with simulations is shown in Figure 3c. The experimental results are taken from Pophel and Fuess.[78] The first three peaks, m (Si−O pair), n (O−O pair), and o (Si−Si pair), correspond to interatomic distances of 1.6, 2.61, and 3.0 Å, respectively. A good match of the first few peaks indicates that the simulated model closely resembles MCM-41 at an atomic level. Although it would not be expected that any kind of ordered silica (α-cristobalite, quartz, or other) will give the same RDF results, Pophal and Fuess[78] reported that the simulated RDF of α-cristobalite matches the experimental MCM-41 results. However, the simulated RDF derived from a cristobalite structure by Fuess and co-workers does not match their experimental RDF as well as the RDF derived from our model does. Specifically, the crstobalite-based model is missing the n peak that is reproduced by our model as seen in Figure 3c.[78] Although the experimentally determined skeletal density of 2.2 g/cm^3 is the same as that of cristobalite (2.2 g/cm^3),[20] there has been no other evidence in the literature that the interstitial structure of MCM-41 has a cristobalite structure.

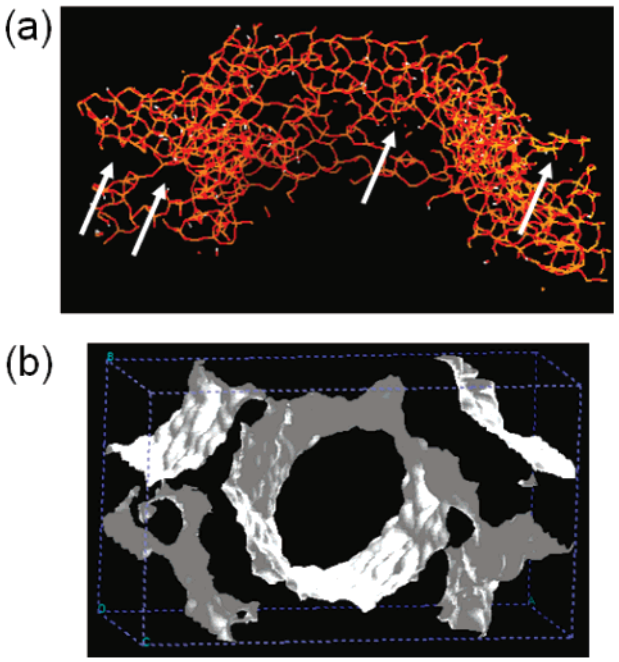

Figure 4. Representation of the surface of MCM-41 developed in the present model including (a) the microscopic deformations in the walls of MCM-41 and (b) the accessible surface area of the model showing microscopic deformations in the walls.

4.3. Accessible Surface Area and Pore Volume. A unit cell of the simulated material showing the deformations in the walls is shown in Figure 4a. The wall deformations were added as described above. The accessible surface area of the structure for penetration of a spherical molecule of 3.8 Å in diameter (effective mean spherical radius of nitrogen based on viscosity measurements[76]) estimated using Connolly surfaces is shown in Figure 4b. The surface area shown represents the surface that is accessible to a spherical probe of diameter 3.68 Å in the periodic cell. For the most part, the surface is accessible through the main cylindrical channel, although there may be small regions on the surface that are buried within the pore walls, representing an experimentally inaccessible surface area. These are likely insignificant, given the wall width and the size of the indentations compared to the accessible surface in the walls due to roughness. The accessible area was found to be 910 m^2/g, whereas the experimental area based on BET measurements for similar materials is in the range of 954−1240 m^2/g, as shown

TABLE 1: Properties of MCM-41 Materials Calculated Using Different Models and Compared with Those from Experimental Results

	surface area (m^2/g)	pore volume (cm^3/g)	lattice parameter (nm)	pore diameter (nm)	area/volume
experimental	960[a]	0.79[a]	4.58	3.5[b]	0.12
geometrical calculations[c]	586	0.51	4.58	3.5	0.12
present model	910	0.72	4.58	3.5	0.13
our results using model of White et al.[32]	257	0.1	4.58	0.7	0.26
our results using model of Koh and co-workers[36]	1117	0.53	4.58	3.5	0.21
our results using model of He and Seaton[38] [d]	280	0.14		3.5	0.2
Maddox et al.[47] [e]	875−956	0.7		4.0	0.13

[a] From the nitrogen adsorption isotherm.[20] [b] Method reported by Kruk et al.[33] was used. [c] Geometrical calculations are based on the smooth cylindrical surface area and a skeletal density of 2.2 g/cm^3. For the 2.85 g/cm^3 density,[47] the surface area is 452 m^2/g, and the pore volume is 0.39 cm^3/g. [d] The model represents MCM-41 as a tube with randomly placed oxygen atoms. [e] The model was not resimulated in the present work.

TABLE 2: BET Surface Areas Calculated Using N_2 Adsorption Isotherms of Representative MCM-41 Materials Synthesized Using C_{16}TMA, Reported in the Literature

area (m^2/g)	reference
954	Ribeiro Carrot et al.[80]
1077	Gubbins et al.[47]
1240	Jaroniec et al.[33]
990	White et al.[32]
1240	Bhatia et al.[17]
910	simulated structure in this work

in Table 1. Figure 4b shows the accessible area of a unit cell with a single cylindrical mesopore at the center, surrounded by one-quarter of the cylindrical pores at each corner. At some places (in Figure 4b), a small connection between two mesopores or an indentation on the surface of mesopores is seen. These indentations do not provide sufficient interconnection between the primary mesopores to claim the occurrence of the interconnecting micropores seen in SBA-15 materials. However, the presence of indentations such as these could certainly be responsible for the increase in accessible surface area beyond the nominal value calculated by assuming that the pores are perfectly smooth. The pore volume using the present model is 0.75 cm^3/g as compared to the experimental value of 0.79 cm^3/g from nitrogen adsorption isotherms.[20,32] While estimating the area by Connolly surfaces, we found that because repetitive estimates of area and volume with the same probe diameter do not differ significantly, the statistical average may not be needed. A more exhaustive statistical analysis would require several structures produced by such a method. We believe that such an exhaustive study would need significant computational time and may not lead to significantly different conclusions.

Assuming a geometry of the unit cell with no physical deformations and a skeletal density of 2.2 g/cm^3, [20] the estimated cell area using perfectly cylindrical pores is 586 m^2/g, and the pore volume is 0.51 cm^3/g. This is sometimes referred to as the estimates by geometric analysis in the literature.[24] Maddox and co-workers[47] reported a skeletal density value between 2.7 and 3.0 g/cm^3, and with that density (2.85 g/cm^3), the geometric area is 452 m^2/g and the pore volume is 0.39 g/cm^3. These geometry-based calculations show a surface area that is significantly lower than the experimental BET area. In addition, the pore volume obtained by nitrogen adsorption (0.79 cm^3/g) is much higher than that obtained by geometric calculations (0.51 cm^3/g). Using similar synthesis procedures, the BET surface areas reported by several investigators for MCM-41, obtained from the literature, are shown in Table 2. It can be seen that they lie between 900 and 1200 m^2/g, which is significantly higher than the geometrical area. Although our present model still slightly underpredicts the surface area reported by several groups for representative MCM-41 samples, the value obtained and the corresponding pore volume are much more realistic than the previous models reported in the literature.

The above data indicate that the present model represents the structure of a typical C_{16}TMA-templated MCM-41 material with reasonable accuracy. However, to determine if the addition of surface heterogeneity makes this model unique, we evaluated other models reported in the literature. In the next section, we study the surface area and pore volume of several structural models reported in the literature.

4.4. Study of Models Reported in the Literature. *Model by White and Co-workers.*[32] It is clear that the samples prepared and reported by White and co-workers[32] are highly ordered because seven diffraction peaks with a small half-peak width can be seen in the original XRD pattern. They[32] carried out a simulation of synchrotron X-ray diffraction patterns of MCM-41 and proposed that MCM-41 had a two-layer wall structure. The inner hollow pore had a radius of 6.89 Å, surrounded by a first layer of wall of 0.87 g/cm^3 density upto the radius of 19.69 Å. The second layer with a density of 0.99 g/cm^3 existed in the rest of the material beyond the radius of 19.69 Å from the center of each pore. To study the proposed model using atomistic simulations, we utilized two approaches. In the first approach, an empty cell of dimensions $7.926 \times 4.577 \times 3$ nm^3 with a cylindrical dummy micelle at the center and four-quarters of the cylindrical dummy micelle at the corners of the cell was created. The Si and O atoms were then randomly placed inside the unit cell using the criteria described in the second approach of the simulation details section above. The sequential placement was stopped when the skeletal density of the first layer between $R_1 = 6.89$ Å and $R_2 = 19.69$ Å was 0.87 g/cm^3 (Figure 1) and the skeletal density of the walls was 0.99 g/cm^3 for $R > 19.69$ Å. The structure was optimized using the procedure described above in section 3.3. In a first approach, where the structure was used without any optimization, the accessible area was found to be 522 m^2/g, as shown in Figure 5a. However, the structure had both accessible and inaccessible micropores. The internal diameter of the main pore was about 6−7 Å, which is significantly lower than the experimentally observed 3.5 nm (estimated from XRD and gas-adsorption studies using the method of Kruk and co-workers[33]). In addition, the structure was not relaxed. Therefore, this approach does not seem to produce a realistic structure. In a second approach, the structure was optimized and equilibrated as discussed in section 3 (method 1) in the simulation details. The accessible area was found to be 257 m^2/g for such a system, as shown in Figure 5b and Table 1. The random surfaces seen in Figure 5b are due to the arrangement of atoms in the model described by the structural model presented in the literature. The surface area is significantly lower than the BET area (990 m^2/g) as well as the geometric area (586 m^2/g). The internal diameter of the main pore in this

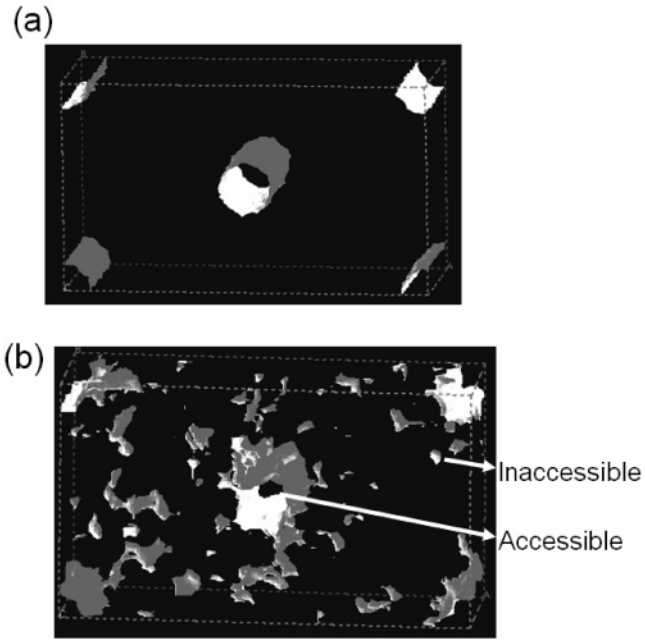

Figure 5. Two-phase wall structure proposed by Edler and co-workers[32] including (a) the unit cell with the two phases, a low-density phase (0.87 g/cm^3) and a higher-density phase (0.99 g/cm^3), (b) the corresponding accessible area in the unoptimized model showing accessible and inaccessible micropores, and (c) the corresponding accessible surface area of the optimized structure.

system was found to be 6.89 Å. Although the structure was relaxed, the internal pore diameter was significantly lower than the experimental observations. The pore volume was found to be 0.1 cm^3/g, which is significantly lower than the experimental value of 0.79 cm^3/g. Therefore, it was found that both of the approaches led to a model that does not predict surface area, pore volume, or pore diameter correctly. On the basis of this, we can conclude that the model proposed by Edler and co-workers[32] underpredicts the surface area and pore volume and it shows what appears to be an unrealistic pore diameter and structure.

Model by Koh and Co-workers.[36,37] The model based on the approach of Koh and co-workers[36,37] is shown in Figure 6a. The accessible surface area by this model, as shown in Figure 4b, was found to be 1117 m^2/g; the pore volume was found to be 0.53 cm^3/g. Although the surface area is comparable and is a good match with experimental values (900−1200 m^2/g), the pore volume is markedly lower than those observed experimentally. In their study of the separation of CH_2Cl_2/N_2, Koh and co-workers[36,37] reported that the model predictions of separation factors were significantly different from the experimental results because of several factors, which include inaccuracies in the structural model as well as force-field parameters. Furthermore, our simulated WAXS results (not shown) of this model have almost no peaks and indicate that the structure has no short-range or long-range order in the walls and therefore does not reasonably represent MCM-41. This is consistent with the discussion in section 2.3 where the model of Koh and co-workers involving the random placement of Si and O atoms was described. Such a structure is not expected to have any crystallinity to be reflected in WAXS patterns.

Estimates of surface area per pore volume (area/volume) are sometimes used to correlate the roughness or tortuosity of a material. The model of Koh and co-workers gives an area/volume that is significantly higher than the experimental values. This higher value indicates that the model generates its high surface area from a high level of microscopic surface roughness due to the random arrangement of atoms and not from more macroscopic indentations in the wall. The accessible surface area as estimated by the Connolly method is shown in Figure 6b.

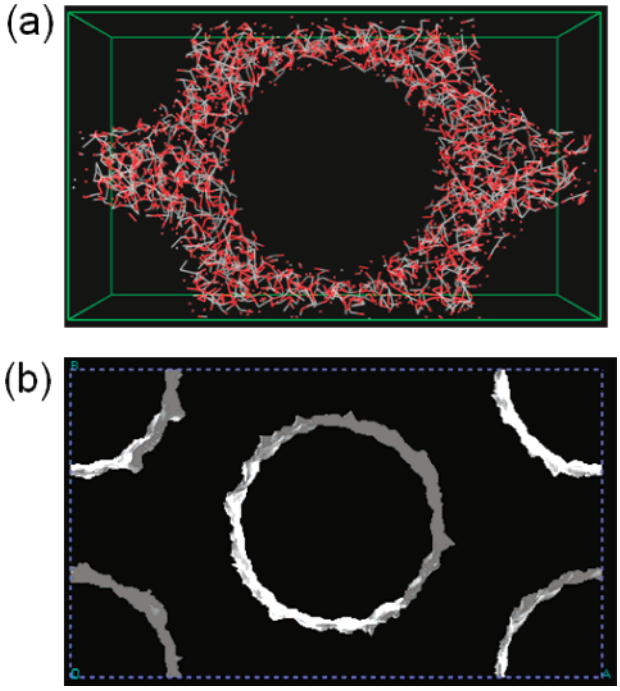

Figure 6. (a) Unit cell of the model proposed by Koh and co-workers[36,37] and (b) the corresponding accessible surface area.

Other Models. The original structural model proposed by Feutson and Higgins[35] was simulated (although different force fields were used). The walls of MCM-41 in their model are similar to vitreous silica (∼2.2−2.4 g/cm^3). The surface area for such a structure was found to be 574 m^2/g, and the pore volume was 0.5 g/cm^3. It can be observed that the surface area and pore volume obtained from their structural model are lower than the experimentally observed BET area and volume.

The model reported by Maddox and Gubbins[47] provides a surface area of 875−965 m^2/g and predicts the pore volume correctly for several MCM-41 samples that they studied. However, their model consists of randomly placed oxygen atoms only (no Si and H atoms) and has a skeletal density of 2.7 g/cm^3, which is higher than that of quartz (2.66 g/cm^3) as well as amorphous silica (2.2 g/cm^3). Of course, for the purpose of modeling gas adsorption, the potential used does not require Si and H atoms. However, our simulated WAXS results of their structure (not shown) do not show any resemblance to experimental results.[78] It may not be realistic to consider a model that consists of randomly placed O atoms hanging in the space for many applications.

The above discussion leads us to conclude that the models in the literature either are too approximate to represent the true structure of MCM-41 or are able to represent the structure up to a certain degree of accuracy but are unable to predict the surface area and pore volume. In addition, none of the models can provide simulated WAXS results that correlate well with experimental results.

4.5. Error in BET Analysis. It is important to point out that it has been argued that the surface area estimated by BET analysis of the isotherm could be inaccurate. In fact, Kruk and co-workers,[24] in one of their early works on MCM-41, suggested the possibility of errors. The BET method estimates the amount

of nitrogen required to fill one monolayer of the adsorbate on the surface of the porous material. Experimental adsorption isotherm data (usually N_2 at 77 K) in the range of ~0.05−0.25 (P/P_0) is used for this purpose. However, a look at the adsorption isotherm of nitrogen on a typical MCM-41 sample shows a pronounced step corresponding to capillary condensation in the range of 0.3−0.4 (P/P_0), very near the ~0.05−0.25 region. In addition, heterogeneity on the surface could lead to a gradual capillary condensation at significantly lower pressures causing the BET surface area to be inaccurate. However, a recent study perhaps provides some answers concerning potential error in the BET area. Galarneau and co-workers[81] reported that the surface area of an 11.5 nm MCM-41 structure is 900 m^2/g. As can be seen from their isotherm, the capillary condensation occurs at approximately 0.85−0.9 P/P_0, which is significantly higher than the pressure range used for the BET analysis of their sample. Therefore, the possibility of errors in surface area due capillary condensation is absent. Thus, for a sample where the likely accuracy of the BET method is high, a very high surface area is still observed. If the BET equation is in fact a reasonable way to represent the surface area of these materials, then the present work provides an alternate model for the structure of MCM-41 that gives simulated surface areas and pore volumes that are in reasonable agreement with experimental surface areas and pore volumes.

5. Conclusions

A new model that more accurately represents the structure of MCM-41 materials was presented. The model is based on the method previously described by Feutson and Higgins, but it incorporates bulk heterogeneity to reproduce the structure of the interstitial silicates between the mesopores. It also incorporates wall indentations to reproduce the effective volume and surface area as characterized by Connolly surfaces. This amorphous structure produces a level of surface roughness that increases the surface area beyond its nominal value, calculated by assuming smooth pores. This model provided the best overall prediction to date of the surface area and volume of the pore structure while also accurately reproducing both representative experimental XRD and WAXS results. We therefore believe that this model represents an accurate model to characterize the interaction of molecules with the pore surface of MCM-41, and we believe that this procedure can be generalized for the simulation of similar mesoporous materials, such as SBA-15.

Acknowledgment. The US DOE Office of Basic Energy Sciences is acknowledged for financial support through Catalysis Science Contract no. DE-FG02-03ER15459. C.G.S. acknowledges Andrew Swann for improvements to the MD code in MOE.

References and Notes

(1) Kresge, C. T.; Roth, W. J.; Vartuli, J. C.; Beck, J. S.; Leonowicz, M. E. *Nature* **1992**, *359*, 710.
(2) Corma, A. *Chem. Rev.* **1997**, *97*, 2373.
(3) Selvam, P.; Bhatia, S. K.; Sonwane, C. G. *Ind. Eng. Chem. Res*. **2001**, *40*, 3237.
(4) Khushalani, D.; Kuperman, A.; Ozin, G. A.; Tanaka, K.; Garces, J.; Olken, M. M.; Coombs, N. *Adv. Mater*. **1995**, 842.
(5) Luechinger, M.; Frunz, L.; Pirngruber, G.; Prins, R. *Microporous Mesoporous Mater*. **2003**, *64*, 203.
(6) Cassiers, K.; Linssen, T.; Mathieu, M.; Benjelloun, M.; Schrijnemakers, K.; Van Der Voort, P.; Cool, P.; Vansant, E. F. *Chem. Mater*. **2002**, *14*, 2317.
(7) Zhang Z.; Han, Y.; Xiao, F. S.; Qiu, S.; Zhu, L.; Wang, R.; Yu, Y.; Zhang, Z.; Zou, B.; Wang, Y.; Sun, H.; Zhao, D.; Wei, Y. *J. Am. Chem. Soc*. **2001**, *123*, 5014.
(8) Beck, J. S.; Vartuli, J. C.; Roth, W. J.; Leonowicz, M. E.; Kresge, C. T.; Schmitt, K. D.; Chu, C. T.-W.; Olsen, D. H.; Sheppard, E. W.; McCullen, S. B.; Higgins, J. B.; Schlenker, J. L. *J. Am. Chem.* Soc. **1992**, *114*, 10 835.
(9) Sano, T.; Doi, K.; Hagimoto, H.; Wang, Z.; Uozumi, T.; Soga, K. *Chem. Commun*. **1999**, *8*, 733.
(10) Wu, C. G.; Bein, T. *Science* **1994**, *266*, 1013.
(11) Kim, S.; Ida, J.; Guliants, V. V.; Lin, Y. S. *Int. J. Environ. Technol. Manage*. **2004**, *4*, 21.
(12) Constantin, C.; Parvulescu, V.; Bujor, A.; Popescu, G.; Su, B. L. *J. Mol. Catal. A*. **2004**, *208*, 245.
(13) Xu, X.; Song, C.; Andresen, J. M.; Miller, B. G.; Scaroni, A. W. *Int. J. Environ. Technol. Manage.* **2004**, *4*, 32.
(14) van der Heijden, A. M.; Lee, T. C.; van Rantwijk, F.; van Bekkum, H. *Carbohydr. Res*. **2002**, *337*, 1993.
(15) Alfredsson, V.; Keung, M.; Monnier, A.; Stucky, G. D.; Unger, K. K.; Schuth, F. *Chem. Commun*. **1994**, 921.
(16) Chen, C. Y.; Xiao, S. Q.; Davis, M. E. *Microporous Mater*. **1993**, *2*, 17.
(17) Sonwane, C. G.; Bhatia, S. K.; Calos, N. *Langmuir* **1999**, *15*, 4603.
(18) Wang, L.-Z.; She, J.-Li.; Tang, F.-Q.; Yu, J.; Ruan, M.-L.; Yan, D.-S. *J. Mater. Chem.* **1999**, *9*, 643.
(19) Fenelonov, V. B.; Derevyankin, A. Yu.; Kirik, S. D.; Solovyov, L. A.; Shmakov, A. N.; Bonardet, J.-L.; Gedeon, A.; Rommanikov, V. N. *Microporous Mesoporous Mater*. **2001**, *44*, 33.
(20) Sonwane, C. G.; Bhatia, S. K.; Calos, N. *Ind. Eng. Chem. Res*. **1998**, *37*, 2271.
(21) Jun, S.; Joo, S. H.; Ryoo, R.; Kruk, M.; Jaroniec, M.; Liu, Z.; Ohsuna, T.; Teresaki, O. *J. Am. Chem. Soc*. **2000**, *122*, 10 712.
(22) Tian, B.; Che, S.; Liu, Z.; Liu, X.; Fan, W.; Tatsumi, T.; Terasaki, O.; Zhao, D. *Chem. Commun.* **2003**, 2726.
(23) Branton, P. J.; Hall P. G.; Sing, K. S. W. *J. Chem. Soc., Chem. Commun*. **1993**, 1257.
(24) Kruk, M.; Jaroniec, M.; Sayari, A. *J. Phys. Chem. B* **1997**, *101*, 583.
(25) Long Y.; Xu, T.; Sun, Y.; Dong, W. *Langmuir* **1998**, *14*, 6173.
(26) Zhao, D.; Huo, Q.; Feng, J.; Chmelka, C. F.; Stucky, G. *J. Am. Chem. Soc*. **1998**, *120*, 6024.
(27) Liu, J.; Zhang, X.; Han, Y.; Xiao, F.-S. *Chem. Mater*. **2002**, *14*, 2536.
(28) Yang, C.-M.; Zibrowius, B.; Schmidt, W.; Schuth, F. *Chem. Mater*. **2004**, *16*, 2918.
(29) Goltner, C. G.; Smarsly, B.; Berton, B.; Antonietti, M. *Chem. Mater*. **2001**, *13*, 1617.
(30) Carr, C. S.; Kaskel, S.; Shantz, D. F. *Chem. Mater*. **2004**, *16*, 3129.
(31) Miyazawa, K.; Inagaki, S. *Chem. Commun*. **2000**, 2121.
(32) Edler, K. J.; Raynolds, P. A.; White, J. W.; Cockson, D. *J. Chem. Soc., Faraday Trans*. **1997**, *93*, 199.
(33) Kruk, M.; Jaroniec, M.; Sayari, A. *J. Phys. Chem. B* **1997**, *101*, 583.
(34) Ravikovitch, P. I.; Wei, D.; Chueh, W. T.; Haller, G. L.; Neimark, A. V. *J. Phys. Chem. B* **1997**, *101*, 3671.
(35) Feutson, B. P.; Higgins, J. B. *J. Phys. Chem*. **1994**, *16*, 4459.
(36) Koh, C. A.; Westacott, R. E.; Nooney, R. I.; Boissel, V.; Tahir, S. F.; Tricarico, V. *Mol. Phys.* **2002**, *100*, 2087.
(37) Koh, C. A.; Montanari, T.; Nooney, R. I.; Tahir, S. F.; Westacott, R. E. *Langmuir* **1999**, *15*, 6043.
(38) He, Y.; Seaton, N. *Langmuir* **2003**, *19*, 10 132.
(39) Yun, J.-H.; Duren, T.; Keil, F. J.; Seaton, N. A. *Langmuir* **2002**, *18*, 2693.
(40) Schacht, S.; Janicke, M.; Schuth, F. *Microporous Mesoporous Mater*. **1998**, *22*, 485.
(41) Solovyov, L. A.; Kirik, S. D.; Shmakov, A. N.; Romannikov, V. N. *Microporous Mesoporous Mater*. **2001**, *44*, 17.
(42) Sauer, J.; Marlow, F.; Schuth, F. *Phys. Chem. Chem. Phys*. **2001**, *3*, 5579.
(43) Kuchta, B.; Llewellyn, P.; Denoyel, R.; Firlej, L. *Colloids Surf., A.* **2004**, *241*, 137.
(44) Cao, D.; Shen, Z.; Chen, J.; Zhang, X. *Microporous Mesoporous Mater.* **2004**, *67*, 159.
(45) Coasne, B.; Pellenq, R. J.-M. *J. Chem. Phys.* **2004**, *120*, 2913.
(46) Kleestorfer, K.; Vinek, H.; Jentys, A. *J. Mol. Catal. A* **2001**, *166*, 53.
(47) Maddox M. W.; Gubbins, K. E. *Langmuir* **1997**, *13*, 1737.
(48) Ravikovitch, P. I.; O'Domhnaill, S. C.; Neimark, A. V.; Schuth, F.; Unger, K. K. *Langmuir* **1995**, *11*, 4765.
(49) Sonwane, C. G.; Bhatia, S. K. *Chem. Eng. Sci*. **1998**, *53*, 3143.
(50) Sonwane, C. G.; Bhatia, S. K. *Langmuir* **1999**, *15*, 2809.
(51) Sonwane, C. G.; Bhatia, S. K. *Langmuir* **1999**, *15*, 5347.
(52) Sonwane, C. G.; Bhatia, S. K. *J. Phys. Chem. B* **2000**, *104*, 9099.
(53) Raja, R.; Thomas, J. M.; Jones, M. D.; Johnson, B. F. G.; Vaughan, D. E. W. *J. Am. Chem. Soc*. **2003**, *125*, 14 982.
(54) Kesanli, B.; Lin, W. B. *Chem. Commun*. **2004**, *20*, 2284.

(55) Li, C. *Catal. Rev. − Sci. Eng*. **2004**, *46*, 419.
(56) McKittrick, M. W.; Jones, C. W. *J. Am. Chem. Soc*. **2004**, *126*, 3052.
(57) Crudden, C. M.; Allen, D.; Mikoluk, M. D.; Sun, J. *Chem. Commun*. **2001**, *13*, 1154.
(58) Hultman, H. M.; de Lang, M.; Nowotny, M.; Arends, I. W. C. E.; Hanefeld, U.; Sheldon, R. A.; Maschmeyer, T. *J. Catal*. **2003**, *217*, 264.
(59) Perez, C.; Perez, S.; Fuentes, G. A.; Corma, A. *J. Mol. Catal. A* **2003**, *197*, 275.
(60) Brunel, D.; Bellocq, N.; Sutra, P.; Cauvel, A.; Lasperas, M.; Moreau, P.; Di Renzo, F.; Galarneau, A.; Fajula, F. *Coord. Chem. Rev.* **1998**, *178*, 1085.
(61) Abrantes, M.; Gago, S.; Valente, A. A.; Pillinger, M.; Goncalves, I. S.; Santos, T. M.; Rocha, J.; Romao, C. C. *Eur. J. Inorg. Chem*. **2004**, *24*, 4914.
(62) Gonzalez-Arellano, C.; Corma, A.; Iglesias, M.; Sanchez, F. *Adv. Synth. Catal*. **2004**, *346*, 1316.
(63) Diaz, J. F.; Balkus, K. J.; Bedioui, F.; Kurshev, V.; Kevan, L. *Chem. Mater*. **1997**, *9*, 61.
(64) Jentys, A.; Kleestorfer, K.; Vinek, H. *Microporous Mesoporous Mater*. **1999**, *27*, 321.
(65) Zhao, X. S.; Lu, G. Q.; Whittaker, A. K.; Miller, G. J.; Zhu, H. Y. *J. Phys. Chem. B* **1997**, *101*, 6525.
(66) *MOE, Molecular Operating Environment*, release 2004.03; Chemical Computing Group Inc.
(67) Gill, P.; Murray W.; Wright, M. *Practical Optimization*; Academic Press: London, 1981.
(68) Halgren, T. A. *J. Comput. Chem*. **1996**, *17*, 490.
(69) Brooks, B. R.; Bruccoleri, R. E.; Olafson, B. D.; States, D. J.; Swaminathan, S.; Karplus, M. *J. Comput. Chem*. **1983**, *4*, 187.
(70) Weiner, S. J.; Kollman, P. A.; Case, D. A.; Singh, U. C.; Ghio, C.; Alagona, G.; Profeta, S.; Weiner, P. *J. Am. Chem. Soc*. **1984**, *106*, 765.
(71) Bond, S. D.; Leimkuhler, B. J.; Laird, B. B. *J. Comput. Phys*. **1999**, *151*, 114.
(72) Sun, G. *J. Comput. Math*. **1993**, *11*, 365.
(73) Allen, M. P.; Tildesly, D. J. *Computer Simulation of Liquids*; Oxford University Press: New York, 1989.
(74) Connolly, M. L. *J. Appl. Crystallogr*. **1983**, *16*, 548.
(75) *Cerius2 Modeling Environment*, release 4.6; Accelrys.
(76) Herschfelder, J. O.; Curtiss, C. F.; Bird, R. B. *Molecular Theory of Gases*; Wiley: New York, 1954.
(77) Ahari, H.; Lough, A.; Petrov, S.; Ozin, G. A.; Bedard, R. L. *J. Mater. Chem*. **1999**, *9*, 1263.
(78) Pophal, C.; Fuess, H. *Microporous Mesoporous Mater*. **1999**, *33*, 241.
(79) Pasuarello, A. *Phys. Rev. B* **2000**, *61*, 3951.
(80) Ribeiro Carrot, M. M. L.; Candeias, A. J. E.; Carrott, P. J. M.; Ravikovitch, P. I.; Neimark, A. V.; Sequeira, A. V. *Microporous Mesoporous Mater*. **2001**, *47*, 323.
(81) Galarneau, A.; Cambon, H.; Renzo, F. D.; Fajula, F. *Langmuir* **2001**, *17*, 8328.